Date of publication xxxx 00, 0000, date of current version xxxx 00, 0000.

Digital Object Identifier 10.1109/ACCESS.2017.DOI

Labelling diversity for media-based space-time block coded spatial modulation

BABATUNDE S. ADEJUMOBI[1] and THOKOZANI SHONGWE [2], (Member, IEEE)

[1]Centre for Telecommunication, Department of Electrical and Electronic Engineering Science, University of Johannesburg, P. O. Box 524 Auckland Park, Johannesburg 2092, South Africa (e-mail: author@lamar.colostate.edu)

[2]Department of Electrical and Electronic Engineering Technology, University of Johannesburg, Doornfontein Campus, Johannesburg 2028, South Africa

Corresponding author: B. S. Adejumobi (e-mail: bsaaadejumobi@uj.ac.za).

This paragraph of the first footnote will contain support information, including sponsor and financial support acknowledgment. For example, "This work was supported in part by the U.S. Department of Commerce under Grant BS123456."

ABSTRACT Media-based space-time block coded spatial modulation (MBSTBC-SM) combines the advantages of media-based modulation (MBM) and STBC-SM. Meanwhile, labelling diversity (LD) has been applied to STBC-SM and improve the error performance. Hence, this paper proposes the application of LD to MBSTBC-SM in the form of MBSTBC-SM-LD over a fast, frequency-flat Rayleigh fading channel, without channel estimation. The proposed MBSTBC-SM-LD demonstrates an improved average bit error rate (BER) performance over MBSTBC-SM and STBC-SM. For example, a 4×4, $n_{rf} = 2$ MBSTBC-SM-LD demonstrates a 2 dB gain in signal-to-noise ratio (SNR) over MBSTBC-SM. Furthermore, the analytical framework for the union bound on the average BER of MBSTBC-SM-LD is formulated, and validates the Monte Carlo simulation results for the MBSTBC-SM system over a fast, frequency-flat Rayleigh fading channel. In addition, a low-complexity detector, which is able to achieve 73% reduction in computational complexity of MBSTBC-SM-LD, while maintaining a near-ML error performance is proposed.

INDEX TERMS labeling diversity, media-based modulation, spatial modulation, space-time block codes, RF mirrors, index modulation,

I. INTRODUCTION

THE 5G and future wireless communication systems require higher data rates, increased spectral efficiency and improved quality of service or link reliability for improved real-time multimedia services. Hence, there has been an upsurge of research focusing on improving pre-existing multiple-input-multiple-output (MIMO) and massive MIMO systems to meet up with these requirements. Some of the schemes that have improved MIMO include the Alamouti space-time block codes (ASTBC) [1]. ASTBC employs two time-slots to transmit two amplitude and/or phase modulation (APM) symbols. The ability for ASTBC to achieve full diversity and employ low-complexity detection has been of immense attraction to researchers [2].

Over the recent years, a new technique known as index modulation, which employs alternative ways than amplitude/frequency/phase to transmit information has gained immense attraction. For example, several schemes, which employ the indexes of the transmit antennas to transmit additional information in the form of index modulation, have been proposed in the literature. These schemes, in contrast with traditional MIMO systems, employ both index modulation and APM symbols to transmit information, hence, improving the spectral efficiency of traditional MIMO.

Spatial modulation (SM) [3], a novel MIMO scheme, which activates a single antenna to transmit an APM symbol in a single time-slot. However, the selected antenna also transmits additional information, thereby improving the spectral efficiency of traditional MIMO. Furthermore, SM is able to reduce power consumption because it employs a single RF chain. Since SM employs a single antenna, it is able to eliminate intersymbol interference and interchannel interference. However, SM is not able to achieve diversity. To remedy this disadvantage, several schemes which employ the principles in SM have been presented in the literature. For example, space-time block coded spatial modulation (STBC-SM) has been proposed in [4]. STBC-SM combines the advantages of ASTBC and SM to improve the error performance of the duo. STBC-SM transmits a pair of APM symbols using two time-slots, through a pair of transmit antennas, which are selected from a set. Furthermore, the computational complexity of the STBC-SM detector is significantly reduced because of the orthogonality of the STBC-SM codeword. To further improve the error performance of SM, labelling diversity (LD) has been applied to STBC-SM in the form of STBC-SM-LD [5]. LD schemes are able to achieve higher diversity gain by employing labelling maps, which maximise the minimum product distance of ASTBC codewords [5]. As recorded in [6], labelling maps eliminate the need for coding or bit interleaving, hence, reducing computational complexity, and ensuring efficient usage of the bandwidth.

A new scheme in wireless communication called Media-based modulation (MBM) [7]–[9] was proposed in the literature. In MBM, information is embedded into the varying number of finite channel states, by changing the RF properties around the transmit antenna, such as (permittivity and permeability) to create different channel realizations. A significant advantage in the application of MBM in wireless communication is that high data rates are achievable, since the constellation size can be increased by varying the channel states. Furthermore, MBM improves error performance because, channel realizations which offer superior error performance can be selected [7], [8].

Whereas radio frequency switches, space shift keying and RF mirrors are some of the methods of MBM presented in the literature [7], [8], [10], employing RF mirror offers a distinct advantage. The spectral efficiency of an RF mirror-based MBM system has a linear relationship with the number of RF mirrors employed for the system. A combination of the ON/OFF status of RF mirrors create distinct channel realizations, which are called mirror activation patterns (MAP). These MAPs are constellations in the spatial domain, hence, increase the spectral efficiency of MBM.

The attractiveness of RF mirror-based MBM (RF-MBM) has resulted in increased interest and focus to this research area. For example, RF mirror was applied to single-input-multiple output in the form of SIMO-MBM and SM in the form of SM-MBM/spatial media-based modulation (SMBM) [8], [10], which resulted in improved spectral efficiency/error performance. Furthermore, MBM has been applied to varying forms of ASTBC. For example, in [10], RF-MBM was applied to ASTBC termed space-time channel modulation (STCM), while a further improvement was achieved in [6] by applying labelling diversity and RF-MBM to ASTBC, in the form of uncoded space-time labelling diversity STCM (USTLD-STCM). In [9], RF-MBM has been applied to STBC-SM and STBC-SM with cyclic structured codeword, in the form of MBSTBC-SM and MBSTBC-CSM, respectively. Three schemes, which are methods used in [6], [11] were applied to MBSTBC-SM and MBSTBC-CSM [9], and achieved significant improvement in error performance when compared to STBC-SM and STBC-CSM, respectively. However, we believe there is still room for improvements in terms of error performance.

Based on the attractiveness of labelling diversity and the application of RF-MBM to STBC-SM, We are motivated to apply the concept of labelling diversity to MBSTBC-SM. Hence, our contributions in this paper are as follows:

1) We propose the application of labelling diversity to MBSTBC-SM, which we have termed MBSTBC-SM-LD to improve the error performance of MBSTBC-SM.
2) We investigate the effect of labelling diversity to the different MAP schemes, which were used in [6], [9], [10], viz; Scheme 1 and 3.
3) A theoretical expression to evaluate the union bound on the average BER of an $N_T \times N_R$ MBSTBC-SM-LD, having m_{rf} RF mirrors, over a fast, frequency-flat, Rayleigh fading channel, where N_T, N_R and m_{rf} are the numbers of transmit antennas, receive antennas and RF mirrors, respectively.
4) The challenge of employing the maximum-likelihood detector is the computational complexity. Hence, we investigate a low complexity detector for MBSTBC-SM-LD, which is independent of the channel fading type (slow or fast fading)

The remainder of this paper is organised as follows: The background of MBSTBC-SM is presented in Section II. The system model of the proposed $N_T \times N_R$ MBSTBC-SM-LD over a fast, frequency-flat Rayleigh fading channel, having m_{rf} RF mirrors is presented in Section III. In Section IV, the theoretical union bound on the average bit error probability for the ML detector of the proposed MBSTBC-SM-LD over an independent and identically distributed (i.i.d.) fast, frequency-flat Rayleigh fading channel is formulated. Section V presents the proposed low-complexity detector for MBSTBC-SM-LD, while in Section VI the analysis of the computational complexities for the different detectors, viz; the ML and low-complexity detectors are analyzed. The Numerical results of the proposed MBSTBC-SM-LD are presented and discussed in Section VII. Finally, this paper is concluded in Section VIII.

Notation: The following notations are employed throughout this paper; bold and capital letters represent matrices, while bold small letters denote column vectors of matrices. Other notations include $(\cdot)^T$ and $(\cdot)^H$ which represent transpose and Hermitian, respectively. $(\cdot)^*$ and $(\cdot)^{-1}$ represent the complex conjugate and inverse, respectively, while $||\cdot||_F$ and $Q(\cdot)$ represent Frobenius norm and Gaussian Q-function, respectively. Furthermore, $\Re(\cdot)$ represents the real part of a complex variable, $\underset{w}{\operatorname{argmin}}(\cdot)$ represents the minimum of an argument with respect to w, and $\binom{\cdot}{\cdot}$ represents the binomial coefficient, $\lfloor w \rfloor_{2p}$ represents the nearest power of two, less than or equal to the w.

II. BACKGROUND OF LABELLING DIVERSITY

This section presents a background of ASTBC and labelling diversity.

STBC employs two time-slots to transmit two symbols. During the first time-slot, the symbols s_1 and s_2, which are selected from an M-ary amplitude and/or phase modulation

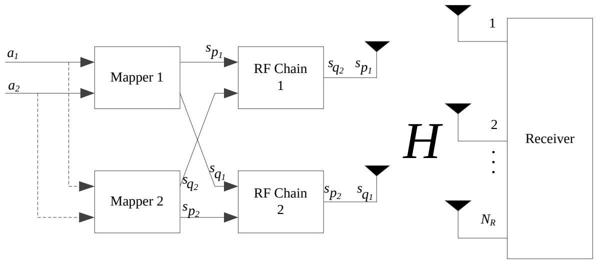

FIGURE 1. System model of a $2 \times N_R$ STLD

(APM) constellation $\mathbf{\Omega}_1$ are transmitted, while in the second time-slot, the conjugates of the symbols transmitted during the first time-slot are transmitted. The transmit codeword of ASTBC may be represented as [1]:

$$\begin{bmatrix} s_p & -s_q^* \\ s_q & s_p^* \end{bmatrix} \tag{1}$$

where s_p and s_q, for $p, q \in [1 : M]$, are the p-th and q-th symbol of the $\mathbf{\Omega}_1$ constellation. M is the constellation size of $\mathbf{\Omega}_1$. Each row in (1) corresponds to the individual transmit antenna and the columns correspond to the time-slots.

Space-time labelling diversity (STLD) is similar to STBC, however, whereas the symbols s_1 and s_2 are taken from the same M-ary APM symbol constellation $\mathbf{\Omega}_1$, the two symbols for STLD are taken from different redesigned M-ary APM optimised constellation sets $\mathbf{\Omega}_1$ and $\mathbf{\Omega}_2$. A $2 \times N_R$ STLD system is as shown in Figure 1, while a pictorial example of 16 QAM labelled mappers, as presented in [12] is given in Figures 2 and 3. The codeword for STLD, may be formulated as:

$$\begin{bmatrix} s_{p_1} & s_{q_2} \\ s_{q_1} & s_{p_2} \end{bmatrix} \tag{2}$$

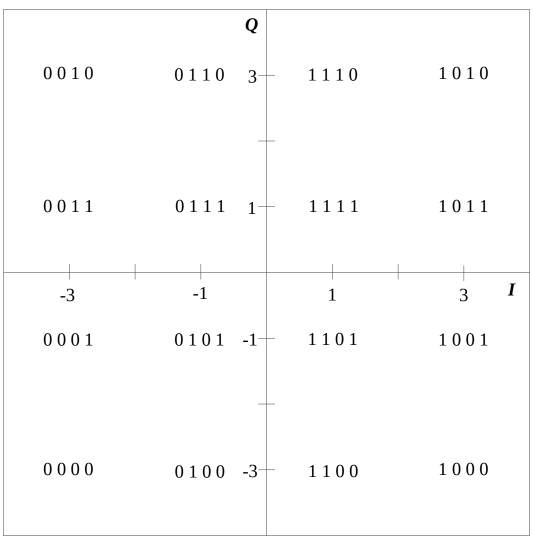

FIGURE 2. Ω_1 labelled map for $M = 16$ [12]

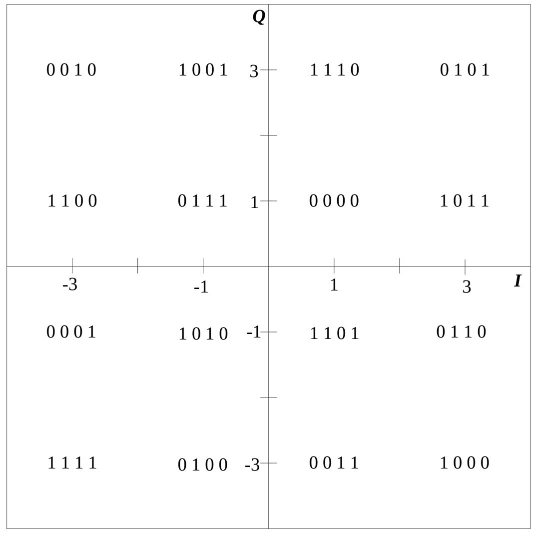

FIGURE 3. Ω_2 labelled map for $M = 16$ [12]

where s_{p_1} and s_{q_1}, for $p_1, q_1 \in [1 : M]$, are the p-th and q-th symbols of $\mathbf{\Omega}_1$ APM symbol mapper, while s_{q_2} and s_{p_2} are the q-th and p-th symbols of $\mathbf{\Omega}_2$ APM symbol mapper, respectively.

III. SYSTEM MODEL OF THE PROPOSED MBSTBC-SM-LD

Given that N_R is the number of receive antennas, and N_T is the number of transmit antennas, this section presents the system model of the proposed $N_R \times N_T$ MBSTBC-SM-LD system. Each transmit antenna of MBSTBC-SM-LD is equipped with m_{rf} RF mirrors as depicted in Figure 4. Furthermore, the transmission of the MBSTBC-SM-LD symbols employ two time-slots, which shall be referred to as Time-slot A and Time-slot B, for the first and second time-slots, respectively.

A group of $\boldsymbol{d}$ bits which is fed into the input of the MBSTBC-SM-LD system is split into three groups, such that $2\log_2 M$ bits are employed to select two symbols from two different M-ary APM symbol mappers. The symbols x_{p_1} and x_{q_1}, where $x_{p_1}, x_{q_1} \in \mathbf{\Omega}_1$, for $p_1, q_1 \in [1 : M]$, are selected from the first APM symbol mapper $\mathbf{\Omega}_1$, such that x_{p_1} and x_{q_1} are the p-th and q-th symbol of $\mathbf{\Omega}_1$. In the same manner, the same bits are employed to select the symbols x_{p_2} and x_{q_2}, where $x_{p_2}, x_{q_2} \in \mathbf{\Omega}_2$, for $p_2, q_2 \in [1 : M]$, which are the p-th and q-th symbol of the second APM symbol mapper $\mathbf{\Omega}_2$. These symbols are transmitted during Time-Slot A, while the conjugates are transmitted during Time-slot B. The second group of bits are the $\log_2 c$, $c = \lfloor 0.5(N_T(N_T-1)) \rfloor_{2p}$ bits, which are employed to select the transmit antenna pair tr_1 and tr_2, where $tr_1, tr_2 \in [1 : N_T]$.

The last (third) group of bits are the $\psi = \gamma m_{rf}$ bits, which are employed to select a MAP of the available $N_m = 2^{m_{rf}}$ MAPs corresponding to each transmit antenna, where γ is a scalar multiplier, which is determined by the scheme

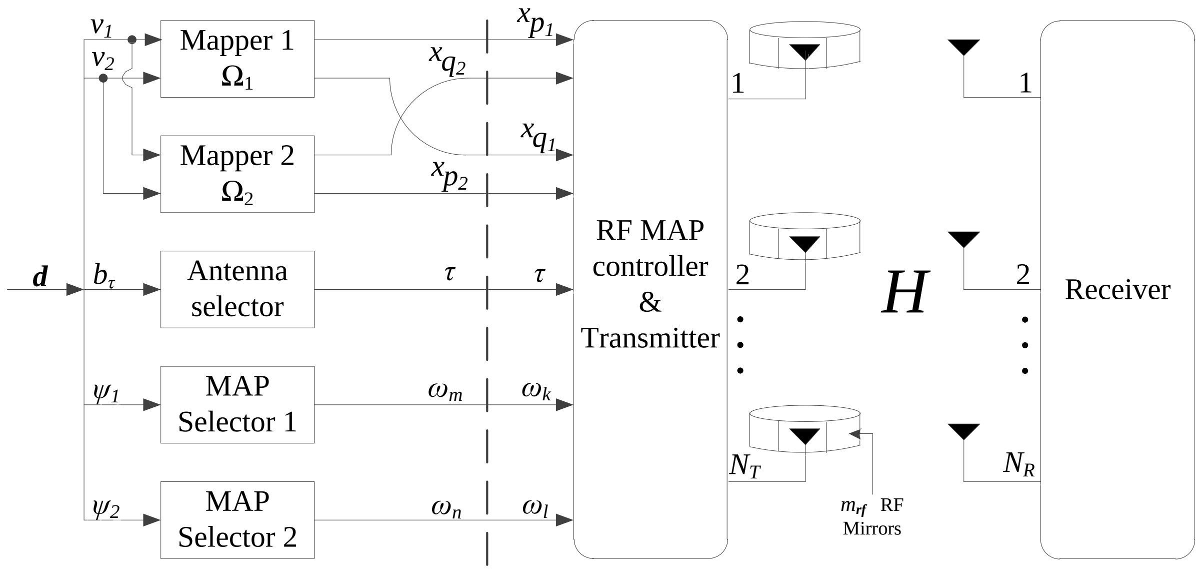

FIGURE 4. System model of an $N_R \times N_T$ m_{rf} MBSTBC-SM-LD.

being used, details of this are given in [9]. For example, in Scheme 2 of [9], where $\gamma = 1$, the ψ bits are used to select a single MAP index, which is employed by all mirrors, while in Scheme 1 and 3, where $\gamma = 2$, the ψ bits are further subdivided into two subgroups, ψ_1 and ψ_2 which are employed to select two different MAPs corresponding to the transmit antenna pair tr_1 and tr_2. The scheme employed determines the MAP arrangement for the first and second time-slot. For time-slot A, the MAPs associated with the transmit antenna pair tr_1 and tr_2, are ω_k and ω_l, respectively, where $\omega_k, \omega_l \in [1 : N_m]$, while the MAPs associated with tr_1 and tr_2 in Time-slot B are ω_m and ω_n, respectively, where $\omega_m, \omega_n \in [1 : N_m]$. Whereas in Scheme 1, $\omega_k = \omega_m$ and $\omega_l = \omega_n$, in Scheme 3, $\omega_k = \omega_n$ and $\omega_l = \omega_m$. In Scheme 2, $\omega_k = \omega_l = \omega_m = \omega_n$. However, we propose the use of Scheme 1 and 3 because of the degraded performance that is offered by Scheme 2 [9].

For more illustration and better understanding, we present an example of bit assignment for the proposed MBSTBC-SM-LD. Given that $N_T = 4$, $M = 4$ and $m_{rf} = 2$ and Scheme 1 is employed for this illustration. From the specification given, it can be deduced that $\gamma = 2$, since we are using Scheme 1, while $c = 4$ and $N_m = 4$. Given that the input bits $\boldsymbol{d}$ of MBSTBC-SM-LD at different transmission times are 0111011000, 1101011001 and 0110000110, the input bit assignment for this scheme can be represented in the format given in Table 1.

Considering the first set of input bits on Row 1 "0111011000", the first group of $2\log_2 M$ bits "0111" are employed to select two symbols x_{p_1} and x_{q_1} from the symbol mapper $\boldsymbol{\Omega}_1$. This is performed by subdividing these bits into two groups $v_1 = 01$ and $v_2 = 11$, such that, v_1 is employed to select the 2-nd symbol x_{2_1} of the first symbol mapper $\boldsymbol{\Omega}_1$, while v_2 is employed to select the 4-th symbol x_{4_1}, of the same symbol mapper $\boldsymbol{\Omega}_1$. These symbols are transmitted in the first time-slot. Conversely, the 2-nd symbol x_{2_2} and the 4-th symbol x_{4_2} of the M-QAM Mapper 2 are transmitted during the second time-slot. Throughout this paper, x_{p_1} and x_{q_1} shall represent the p-th and q-th symbol of the M-QAM Mapper 1, while x_{p_2} and x_{q_2} shall represent p-th and q-th symbols of the M-QAM Mapper 2.

The second group of the $\boldsymbol{d}$ bits $b_\tau = 01$, are the next $\log_2 c$ bits, which determines the transmit antenna pair, that will be employed to transmit the selected symbols. For $N_T = 4$, the c transmit antenna pairs (tr_1, tr_2) are $(1,2)$, $(3,4)$, $(1,4)$ and $(2,3)$. Hence, the τ-th transmit pair that will be selected by the b_τ bits is $(3,4)$. Finally, the third group of bits, are the $\psi = 1000$ bits, which is further subdivided into $\psi_1 = 10$ and $\psi_2 = 00$ bits, which are employed to select the MAP to be activated during transmission. The ψ_1 and ψ_2 bits are employed to activate the $\omega_k = 3$-rd and $\omega_l = 1$-st MAPs of the RF mirrors on the 3-rd and 4-th transmit antennas, respectively.

The bit assignment for Scheme 3 follows the same method as Scheme 1 during the first time-slot, However, in the second time-slot, there are changes made to the MAP indices. Whereas $\omega_k = \omega_m$ and $\omega_l = \omega_n$ in Scheme 1, $\omega_k = \omega_n$ and $\omega_l = \omega_m$ in Scheme 3. Hence, using the same input bits as that in Table 1, the bit assignment for Scheme 3 is as shown in Table 2

The received signal matrix $\boldsymbol{Y}$ at the receiver of the MBSTBC-SM-LD system may be represented as:

$$\boldsymbol{Y} = [\boldsymbol{y}_A \quad \boldsymbol{y}_B] = \sqrt{\frac{\rho}{2}}\,[\boldsymbol{H}^A \boldsymbol{u}_A \quad \boldsymbol{H}^B \boldsymbol{u}_B] + \boldsymbol{N} \tag{3}$$

where $\boldsymbol{Y} = [\boldsymbol{y}_A \quad \boldsymbol{y}_B]$ is an $N_R \times 2$ matrix having each

TABLE 1. Bit assignments for Scheme 1

Row	d Bits	v_1	p	v_2	q	b_τ	τ	ψ_1	ω_k	ψ_2	ω_l	ω_m	ω_n
1	01 11 01 10 00	01	2	11	4	01	2	10	3	00	1	3	1
2	11 01 01 10 01	11	4	01	2	01	2	10	3	01	2	3	2
3	01 10 00 01 10	01	2	10	3	00	1	01	2	10	3	2	3

TABLE 2. Bit assignments for Scheme 3

Row	d Bits	v_1	p	v_2	q	b_τ	τ	ψ_1	ω_k	ψ_2	ω_l	ω_m	ω_n
1	01 11 01 10 00	01	2	11	4	01	2	10	3	00	1	1	3
2	11 00 01 11 01	11	4	00	1	01	2	11	4	01	2	2	4
3	01 10 00 10 10	01	2	10	3	00	1	10	3	10	3	3	3

column representing the signal vector for each time-slot, viz; Time-slot A and B. $\boldsymbol{u}_A$ is an $N_T N_m \times 1$ transmit vector for Time-slot A , having the symbols x_{p_1} and x_{q_1} as the only non-zero entry on the t_{p_a}-th, $t_{p_a} = N_m(tr_1 - 1) + \omega_k$ and t_{q_a}-th, $t_{q_a} = N_m(tr_2 - 1) + \omega_l$ position, respectively. Conversely, $\boldsymbol{u}_B$ is an $N_T N_m \times 1$ transmit vector for Time-slot B, having the symbols x_{q_2} and x_{p_2} as the only non-zero entry on the t_{q_b}-th, $t_{q_b} = N_m(tr_1 - 1) + \omega_m$ and t_{p_b}-th, $t_{p_b} = N_m(tr_2 - 1) + \omega_n$ position, respectively. The transmit codeword matrix $\boldsymbol{U} = \begin{bmatrix}\boldsymbol{u}_A & \boldsymbol{u}_B\end{bmatrix}$ for the proposed MBSTBC-SM-LD system is similar to the codeword matrix given in [4]. However, whereas the transmit codeword matrix for STBC-SM is an $N_T \times 2$ matrix, MBSTBC-SM-LD employs an $N_T N_m \times 2$ codeword matrix.

The channel matrix $\boldsymbol{H}^A$ and $\boldsymbol{H}^B$ is each defined as an $N_R \times N_T N_m$ tuple channel matrix, where $\sqrt{\frac{\rho}{2}}\boldsymbol{H}^A = \begin{bmatrix}\boldsymbol{H}_1^A & \boldsymbol{H}_2^A & \cdots & \boldsymbol{H}_{N_T}^A\end{bmatrix}^T$ and $\sqrt{\frac{\rho}{2}}\boldsymbol{H}^B = \begin{bmatrix}\boldsymbol{H}_1^B & \boldsymbol{H}_2^B & \cdots & \boldsymbol{H}_{N_T}^B\end{bmatrix}^T$. The noise at the receiver $\boldsymbol{N} = \begin{bmatrix}\boldsymbol{n_A} & \boldsymbol{n_B}\end{bmatrix}$ is defined as an $N_R \times 2$ additive white Gaussian noise (AWGN) matrix, whose entries are independent and identically distributed (i.i.d.) with zero mean and unit variance $CN(0,1)$. ρ is defined as the average signal-to-noise ratio at the receiver.

A simplified form of (3), for the received signal vectors $\boldsymbol{y}_A$ and $\boldsymbol{y}_B$ of MBSTBC-SM-LD over a fast frequency-flat Rayleigh fading channel for two time-slots; viz, times-slots A and B, may be written as [9]:

$$\boldsymbol{y}_A = \sqrt{\frac{\rho}{2}}\boldsymbol{H}_{tr_1}^A x_{p_1}\boldsymbol{e}_{\omega_k} + \sqrt{\frac{\rho}{2}}\boldsymbol{H}_{tr_2}^A x_{q_1}\boldsymbol{e}_{\omega_l} + \boldsymbol{n}_A \quad (4)$$

$$\boldsymbol{y}_B = \sqrt{\frac{\rho}{2}}\boldsymbol{H}_{tr_1}^B x_{q_2}\boldsymbol{e}_{\omega_m} + \sqrt{\frac{\rho}{2}}\boldsymbol{H}_{tr_2}^B x_{p_2}\boldsymbol{e}_{\omega_n} + \boldsymbol{n}_B \quad (5)$$

where $\boldsymbol{H}_{tr_1}^A$ and $\boldsymbol{H}_{tr_2}^A$, for $tr_1, tr_2 \in [1 : N_T]$, are each the $N_R \times N_m$ tuple channel matrix for the transmit antenna pair tr_1 and tr_2, employed during time-slot A, respectively, while $\boldsymbol{H}_{tr_1}^B$ and $\boldsymbol{H}_{tr_2}^B$ are each the $N_R \times N_m$ channel matrix for the transmit antenna pair tr_1 and tr_2, employed in time-slot B, respectively. $\boldsymbol{n}_A$ and $\boldsymbol{n}_B$ are each an $N_R \times 1$ i.i.d AWGN vector having $\boldsymbol{CN}(0,1)$ distribution for time-slot A and time-slot B, where $\boldsymbol{n}_\beta = \begin{bmatrix}n_{\beta,1} & n_{\beta,2} & \cdots & n_{\beta,N_R}\end{bmatrix}^T$, for $\beta \in \{A, B\}$. $\boldsymbol{H}_{tr_\alpha}^i = \begin{bmatrix}\boldsymbol{h}_{tr_\alpha,1}^i & \boldsymbol{h}_{tr_\alpha,2}^i & \cdots & \boldsymbol{h}_{tr_\alpha,N_m}^i\end{bmatrix}$, for $\alpha \in [1 : 2]$ and $i \in \{A, B\}$. Each vector of $\boldsymbol{H}_{tr_\alpha}^i$ can be defined by $\boldsymbol{h}_{tr_\alpha}^{i,\psi} = \begin{bmatrix}h_{tr_\alpha,1}^{i,\psi} & h_{tr_\alpha,2}^{i,\psi} & \cdots & h_{tr_\alpha,N_R}^{i,\psi}\end{bmatrix}^T$, for $\psi \in [1 : N_m]$. The vectors $\boldsymbol{e}_{\omega_k}$ and $\boldsymbol{e}_{\omega_l}$ are each an $N_m \times 1$ vector having the ω_k-th and ω_l-th element, respectively, as unity during the first time-slot while $\boldsymbol{e}_{\omega_m}$ and $\boldsymbol{e}_{\omega_n}$ are each an $N_m \times 1$ vector having the ω_m-th and ω_n-th element, respectively, as unity during the second time-slot. Hence, a simplified form for the received signal vector for time-slots A and B given in (4) and (5) respectively, of the proposed MBSTBC-SM-LD is formulated as [9]:

$$\boldsymbol{y}_A = \boldsymbol{h}_{tr_1,\omega_k}^A x_{p_1} + \boldsymbol{h}_{tr_2,\omega_l}^A x_{q_1} + \boldsymbol{n}_A \quad (6)$$

$$\boldsymbol{y}_B = \boldsymbol{h}_{tr_1,\omega_m}^B x_{q_2} + \boldsymbol{h}_{tr_2,\omega_n}^B x_{p_2} + \boldsymbol{n}_B \quad (7)$$

From (4) and (5), the joint maximum-likelihood (ML) detector for the received signal vector of MBSTBC-SM-LD may be formulated as:

$$\begin{aligned}&\begin{bmatrix}\hat{\tau}, & \hat{\omega}_k, & \hat{\omega}_l, & \hat{p}_1, & \hat{q}_2\end{bmatrix} \\ &= \underset{\substack{\tau\in[1:c] \\ \omega_k,\omega_l\in[1:N_m] \\ p_1,q_2\in[1:M]}}{\operatorname{argmin}} \left\{\left\|\boldsymbol{y}_A - \sqrt{\frac{\rho}{2}}\left(\boldsymbol{H}_{tr_1}^A x_{p_1}\boldsymbol{e}_{\omega_k} + \boldsymbol{H}_{tr_2}^A x_{q_1}\boldsymbol{e}_{\omega_l}\right)\right\|_F^2\right. \\ &\left. + \left\|\boldsymbol{y}_B - \sqrt{\frac{\rho}{2}}\left(\boldsymbol{H}_{tr_1}^B x_{q_2}\boldsymbol{e}_{\omega_m} + \boldsymbol{H}_{tr_2}^B x_{p_2}\boldsymbol{e}_{\omega_n}\right)\right\|_F^2\right\} \quad (8)\end{aligned}$$

while the reduced form may be represented as:

$$\begin{aligned}&\begin{bmatrix}\hat{\tau}, & \hat{\omega}_k, & \hat{\omega}_l, & \hat{p}_1, & \hat{q}_2\end{bmatrix} \\ &= \underset{\substack{\tau\in[1:c] \\ \omega_k,\omega_l\in[1:N_m] \\ p_1,q_2\in[1:M]}}{\operatorname{argmin}} \left\{\left\|\boldsymbol{y}_A - \left(\boldsymbol{h}_{tr_1,\omega_k}^A x_{p_1} + \boldsymbol{h}_{tr_2,\omega_l}^A x_{q_1}\right)\right\|_F^2\right. \\ &\left. + \left\|\boldsymbol{y}_B - \left(\boldsymbol{h}_{tr_1,\omega_m}^B x_{q_2} + \boldsymbol{h}_{tr_2,\omega_n}^B x_{p_2}\right)\right\|_F^2\right\} \quad (9)\end{aligned}$$

where $\hat{\tau}$, $\hat{\omega}_k$, $\hat{\omega}_l$, $\hat{p}_1$ and $\hat{q}_2$ are estimates of τ, ω_k, ω_l, p_1 and q_2, respectively.

A reduced form of (8), which will be employed to calculate the computational complexity of MBSTBC-SM-LD may be represented as [9]:

$$\begin{aligned}&[\hat{\tau},\quad \hat{\omega}_k,\quad \hat{\omega}_l,\quad \hat{p}_1,\quad \hat{q}_2]\\&\quad=\underset{\substack{\tau\in[1:c],\ \omega_k,\omega_l\in[1:N_m]\\ p_1,q_2\in[1:M]}}{\operatorname{argmin}}\Big\{\|\boldsymbol{g}_{p_1}^k\|_F^2+\|\boldsymbol{g}_{q_1}^l\|_F^2\\&\quad-2\Re\left(\boldsymbol{y}_A^H\boldsymbol{g}_{p_1}^k\right)-2\Re\left(\boldsymbol{y}_A^H\boldsymbol{g}_{q_1}^l\right)+\Re\left(\left(\boldsymbol{g}_{p_1}^k\right)^H\boldsymbol{g}_{q_1}^l\right)\\&\quad+\|\boldsymbol{g}_{q_2}^m\|_F^2+\|\boldsymbol{g}_{p_2}^n\|_F^2-2\Re\left(\boldsymbol{y}_B^H\boldsymbol{g}_{q_2}^m\right)-2\Re\left(\boldsymbol{y}_B^H\boldsymbol{g}_{p_2}^n\right)\\&\quad+\Re\left(\left(\boldsymbol{g}_{q_2}^m\right)^H\boldsymbol{g}_{p_2}^n\right)\Big\}\end{aligned}\qquad(10)$$

where $\boldsymbol{g}_{p_1}^k=\boldsymbol{h}_{tr_1,\omega_k}^A x_{p_1}$, $\boldsymbol{g}_{q_1}^l=\boldsymbol{h}_{tr_2,\omega_l}^A x_{q_1}$, $\boldsymbol{g}_{q_2}^m=\boldsymbol{h}_{tr_1,\omega_m}^B x_{q_2}$ and $\boldsymbol{g}_{p_2}^n=\boldsymbol{h}_{tr_2,\omega_n}^B x_{p_2}$.

IV. ANALYTICAL ABEP OF MBSTBC-SM-LD

In this section, the analytical ABEP of MBSTBC-SM-LD is formulated for a fast, frequency-flat Rayleigh fading channel.

The ABEP of MBSTBC-SM-LD is defined as [9]:

$$ABEP\le E\left[\sum_{\boldsymbol{U}}\sum_{\hat{\boldsymbol{U}}}N_{\boldsymbol{U}\hat{\boldsymbol{U}}}P\left(\boldsymbol{U}\rightarrow\hat{\boldsymbol{U}}\right)\right]\qquad(11)$$

where E $[\cdot]$ is the expectation.

$$\begin{aligned}&ABEP\\&\le\frac{1}{cN_m^2M^2}\sum_{\boldsymbol{U}}\sum_{\hat{\boldsymbol{U}}}\frac{N_{\boldsymbol{U}\hat{\boldsymbol{U}}}P\left(\boldsymbol{U}\rightarrow\hat{\boldsymbol{U}}\right)}{(\log_2c+\log_2M^2+\log_2N_m^2)}\end{aligned}\qquad(12)$$

$$\begin{aligned}&ABEP\\&\le\sum_{\tau=1}^{c}\sum_{\tau=1}^{c}\sum_{p_1=1}^{M}\sum_{q_1=1}^{M}\sum_{\hat{p}_1=1}^{M}\sum_{\hat{q}_1=1}^{M}\sum_{\omega_k=1}^{N_m}\sum_{\omega_l=1}^{N_m}\sum_{\hat{\omega}_k=1}^{N_m}\\&\sum_{\hat{\omega}_l=1}^{N_m}\left(\frac{N_{\boldsymbol{U}\hat{\boldsymbol{U}}}P\left(\boldsymbol{U}\rightarrow\hat{\boldsymbol{U}}\right)}{(\log_2c+\log_2M^2+\log_2N_m^2)}\right)\end{aligned}\qquad(13)$$

where $P\left(\boldsymbol{U}\rightarrow\hat{\boldsymbol{U}}\right)$ is the pair error wise probability (PEP) event, given that $\boldsymbol{U}$ is the transmit codeword matrix of the form defined in (3), which is erroneously decided by the receiver as $\hat{\boldsymbol{U}}$. $N_{\boldsymbol{U}\hat{\boldsymbol{U}}}$ is the number of bits received in error, given that the PEP event $P\left(\boldsymbol{U}\rightarrow\hat{\boldsymbol{U}}\right)$ has occurred.

Considering $\boldsymbol{H}_\tau^A=[\boldsymbol{H}_{tr_1}^A\ \ \boldsymbol{H}_{tr_2}^A]$, $\boldsymbol{H}_\tau^B=[\boldsymbol{H}_{tr_1}^B\ \ \boldsymbol{H}_{tr_2}^B]\in\boldsymbol{H}$, the conditional probability $P\left(\boldsymbol{U}\rightarrow\hat{\boldsymbol{U}}\mid\boldsymbol{H}\right)$ may be formulated as [4]:

$$\begin{aligned}&P\left(\boldsymbol{U}\rightarrow\hat{\boldsymbol{U}}\mid\boldsymbol{H}\right)=\\&P\Bigg(\left\|\boldsymbol{y}_A-\sqrt{\frac{\rho}{2}}\left(\boldsymbol{H}_{tr_1}^A x_{p_1}\boldsymbol{e}_{\omega_k}+\boldsymbol{H}_{tr_2}^A x_{q_1}\boldsymbol{e}_{\omega_l}\right)\right\|_F^2\\&+\left\|\boldsymbol{y}_B-\sqrt{\frac{\rho}{2}}\left(\boldsymbol{H}_{tr_1}^B x_{q_2}\boldsymbol{e}_{\omega_m}+\boldsymbol{H}_{tr_2}^B x_{p_2}\boldsymbol{e}_{\omega_n}\right)\right\|_F^2\\&>\left\|\boldsymbol{y}_A-\sqrt{\frac{\rho}{2}}\left(\boldsymbol{H}_{\hat{t}r_1}^A x_{\hat{p}_1}\boldsymbol{e}_{\hat{\omega}_k}+\boldsymbol{H}_{\hat{t}r_2}^A x_{\hat{q}_1}\boldsymbol{e}_{\hat{\omega}_l}\right)\right\|_F^2\\&+\left\|\boldsymbol{y}_B-\sqrt{\frac{\rho}{2}}\left(\boldsymbol{H}_{\hat{t}r_1}^B x_{\hat{q}_2}\boldsymbol{e}_{\hat{\omega}_m}+\boldsymbol{H}_{\hat{t}r_2}^B x_{\hat{p}_2}\boldsymbol{e}_{\hat{\omega}_n}\right)\right\|_F^2\Bigg)\end{aligned}\qquad(14)$$

From [6], [12] , the reduced form of (14) may be formulated as:

$$\begin{aligned}&P\left(\boldsymbol{U}\rightarrow\hat{\boldsymbol{U}}\mid\boldsymbol{H}\right)\\&=Q\left(\sqrt{\frac{\rho}{8}\left\|\boldsymbol{H}_{12}^A\right\|_F^2\left\|\boldsymbol{u}_{A\hat{A}}\right\|_F^2+\frac{\rho}{8}\left\|\boldsymbol{H}_{12}^B\right\|_F^2\left\|\boldsymbol{u}_{B\hat{B}}\right\|_F^2}\right)\\&=Q\left(\sqrt{k_A+k_B}\right)\end{aligned}\qquad(15)$$

where $\boldsymbol{u}_{A\hat{A}}=\boldsymbol{U}_A-\hat{\boldsymbol{U}}_A$, $\boldsymbol{U}_A$ and $\hat{\boldsymbol{U}}_A$ are the A-th $N_TN_m\times1$ column vectors, representing the first time-slots of $\boldsymbol{U}$ and $\hat{\boldsymbol{U}}$, respectively. Furthermore, $\boldsymbol{u}_{B\hat{B}}=\boldsymbol{U}_B-\hat{\boldsymbol{U}}_B$, $\boldsymbol{U}_B$ and $\hat{\boldsymbol{U}}_B$ are the B-th $N_TN_m\times1$ column vectors, representing the second time-slots of $\boldsymbol{U}$ and $\hat{\boldsymbol{U}}$, respectively. Hence the unconditional PEP can be obtained by averaging the conditional PEP $P\left(\boldsymbol{U}\rightarrow\hat{\boldsymbol{U}}\mid\boldsymbol{H}\right)$ which may be formulated as [12]:

$$P\left(\boldsymbol{U}\rightarrow\hat{\boldsymbol{U}}\right)=\int_0^\infty\int_0^\infty Q\left(\sqrt{k_A+k_B}\right)f_{k_A}f_{k_B}d\theta_1d\theta_2\qquad(16)$$

where f_{k_A} and f_{k_B} are the probability density functions of k_A and k_B, respectively, which follows a Rayleigh distribution.

To simplify the expression in (16), the exponential expression of Q-function is employed by applying the trapezoidal approximation definition of $Q(\sqrt{x})$ and is defined as:

$$\begin{aligned}&Q\left(\sqrt{k_A+k_B}\right)\\&=\frac{1}{2a}\left[\frac{1}{2}e^{\left(-\frac{k_A}{2}\right)}e^{\left(-\frac{k_B}{2}\right)}+\sum_{g=1}^{a-1}e^{\left(-\frac{k_A}{2\sin^2\theta_g}\right)}e^{\left(-\frac{k_B}{2\sin^2\theta_g}\right)}\right]\end{aligned}\qquad(17)$$

Applying the trapezoidal approximation rule to the Q-function of (15), it becomes [13]:

$$P\left(\boldsymbol{U} \rightarrow \hat{\boldsymbol{U}}\right) = \frac{1}{2a}\left[\frac{1}{2} M_A\left(\frac{1}{2}\right) M_B\left(\frac{1}{2}\right) + \sum_{g=1}^{a-1} M_A\left(\frac{1}{2\sin^2\theta_g}\right) M_B\left(\frac{1}{2\sin^2\theta_g}\right)\right] \quad (18)$$

where $M_A(w) = \left(1+2\sigma^2_{\alpha_A} w\right)^{-N_R}$, $M_B(w) = \left(1+2\sigma^2_{\alpha_B} w\right)^{-N_R}$, $\sigma^2_{\alpha_A} = \frac{\rho}{8}\left\|\boldsymbol{u}_{A\hat{A}}\right\|^2_F$, $\sigma^2_{\alpha_B} = \frac{\rho}{8}\left\|\boldsymbol{u}_{B\hat{B}}\right\|^2_F$ and $\theta_g = \frac{\pi g}{2a}$, where a is the number of iterations needed for convergence of the Q-function, when the trapezoidal approximation is employed.

V. LOW-COMPLEXITY NEAR-ML DETECTOR FOR MBSTBC-SM-LD

The computational complexity for MBSTBC-SM-LD is very large, because the computation/search algorithm parses large amount of data as would be shown in the next section. Hence, in this section, we propose an orthogonal projection-based low-complexity detector for MBSTBC-SM-LD.

We consider the MBSTBC-SM-LD system, having N_R receive antennas, N_T transmit antennas and m_{rf} RF mirrors associated with each transmit antenna. The proposed low-complexity near-ML detector for MBSTBC-SM-LD determine the f_1 and f_2 nearest estimates $\boldsymbol{u}^p = [u_1 \ \ u_2 \ \ \cdots \ \ u_{f_1}]$ and $\boldsymbol{u}^q = [u_1 \ \ u_2 \ \ \cdots \ \ u_{f_2}]$, which are the indexes of the nearest estimates of transmitted symbols p and q, $p, q \in [1 : M]$, for all the c antenna pairs (tr_1, tr_2), $tr_1, tr_2 \in [1 : N_T]$, such that $tr_1 \neq tr_2$ and $f_1 f_2 \ll M^2$.

To determine the indexes of the most likely candidate set of the transmitted symbols, the orthogonal projection matrices $\boldsymbol{P}^A_{tr_a,\omega_b}$ and $\boldsymbol{P}^B_{tr_a,\omega_b}$, where $a \in [1 : 2]$ and $\omega_b \in [1 : Nm]$ corresponding to the channel subspace $\boldsymbol{h}^A_{tr_a,\omega_b}$ and $\boldsymbol{h}^B_{tr_a,\omega_b}$, respectively, are computed, such that $\boldsymbol{P}^A_{tr_a,\omega_b}\boldsymbol{h}^A_{tr_a,\omega_b} = \boldsymbol{P}^B_{tr_a,\omega_b}\boldsymbol{h}^B_{tr_a,\omega_b} = 0$. $\boldsymbol{P}^A_{tr_a,\omega_b}$ and $\boldsymbol{P}^B_{tr_a,\omega_b}$ are defined in (19) and (20) as [5], [9]:

$$\boldsymbol{P}^A_{tr_a,\omega_b} = \boldsymbol{I}_{N_R} - \boldsymbol{h}^A_{tr_a,\omega_b}\left(\left(\boldsymbol{h}^A_{tr_a,\omega_b}\right)^H \boldsymbol{h}^A_{tr_a,\omega_b}\right)^{-1}\left(\boldsymbol{h}^A_{tr_a,\omega_b}\right)^H \quad (19)$$

$$\boldsymbol{P}^B_{tr_a,\omega_b} = \boldsymbol{I}_{N_R} - \boldsymbol{h}^B_{tr_a,\omega_b}\left(\left(\boldsymbol{h}^B_{tr_a,\omega_b}\right)^H \boldsymbol{h}^B_{tr_a,\omega_b}\right)^{-1}\left(\boldsymbol{h}^B_{tr_a,\omega_b}\right)^H \quad (20)$$

where $\boldsymbol{P}^A_{tr_a,\omega_b}$ and $\boldsymbol{P}^B_{tr_a,\omega_b}$ are the projection matrices for the time-slots A and B, respectively, given that the tr_a-th, $a \in [1 : 2]$ transmit antenna has been employed, while the ω_b-th MAP has been activated.

If $\hat{z}^q_{u_1} = x_{q_1}$ and $\hat{z}^q_{u_2} = x_{q_2}$, where $u_1 \in [1 : f_1]$, $u_2 \in [1 : f_2]$, $u_1, u_2 \subseteq [1 : M]$, $\hat{z}^q_{u_1} \subseteq \boldsymbol{\Omega}_1$ and $\hat{z}^q_{u_2} \subseteq \boldsymbol{\Omega}_2$ then, the sum of the projections can be formulated as [5], [9], [14]:

$$\boldsymbol{P}^A_{tr_1,\omega_k}\boldsymbol{r}^{A,q}_{tr_2,\omega_l} + \boldsymbol{P}^B_{tr_2,\omega_n}\boldsymbol{r}^{B,q}_{tr_1,\omega_m} = \boldsymbol{P}^A_{tr_1,\omega_k}\boldsymbol{n}_A + \boldsymbol{P}^B_{tr_2,\omega_n}\boldsymbol{n}_B \quad (21)$$

where $\boldsymbol{r}^{A,q}_{tr_2,\omega_l}$ and $\boldsymbol{r}^{B,q}_{tr_1,\omega_m}$ are the projection spaces corresponding to the projection matrices in $\boldsymbol{P}^A_{tr_1,\omega_k}$ and $\boldsymbol{P}^B_{tr_2,\omega_n}$, respectively, and are defined in (22) and (23), respectively as:

$$\boldsymbol{r}^{A,q}_{tr_2,\omega_l} = \boldsymbol{y}_A - \sqrt{\frac{\rho}{2}}\boldsymbol{h}^A_{tr_2,\omega_l}\hat{z}^q_{u_1} \quad (22)$$

$$\boldsymbol{r}^{B,q}_{tr_1,\omega_m} = \boldsymbol{y}_B - \sqrt{\frac{\rho}{2}}\boldsymbol{h}^B_{tr_1,\omega_m}\hat{z}^q_{u_2} \quad (23)$$

however, if $\hat{z}^q_{u_1} \neq x_{q_1}$ and $\hat{z}^q_{u_2} \neq x_{q_2}$, (21) yields [5], [9], [14]:

$$\sqrt{\frac{\rho}{2}}\boldsymbol{P}^A_{tr_1,\omega_k}\boldsymbol{h}^A_{tr_2,\omega_l}\left(x_{q_1} - \hat{z}^q_{u_1}\right) + \boldsymbol{P}^B_{tr_2,\omega_n}\boldsymbol{h}^B_{tr_1,\omega_m}\left(x_{q_2} - \hat{z}^q_{u_2}\right) + \boldsymbol{P}^A_{tr_1,\omega_k}\boldsymbol{n}_A + \boldsymbol{P}^B_{tr_2,\omega_n}\boldsymbol{n}_B \quad (24)$$

In the same manner as (21), if $\hat{z}^p_{u_1} = x_{p_1}$ and $\hat{z}^p_{u_2} = x_{p_2}$, where $u_1 \in [1 : f_1]$ and $u_2 \in [1 : f_2]$, then, the sum of the projections can be formulated as [5], [9], [14]:

$$\boldsymbol{P}^A_{tr_2,\omega_l}\boldsymbol{r}^{A,p}_{tr_1,\omega_k} + \boldsymbol{P}^B_{tr_1,\omega_m}\boldsymbol{r}^{B,p}_{tr_2,\omega_n} = \boldsymbol{P}^A_{tr_2,\omega_l}\boldsymbol{n}_A + \boldsymbol{P}^B_{tr_1,\omega_m}\boldsymbol{n}_B \quad (25)$$

where $\boldsymbol{r}^{A,p}_{tr_1,\omega_k}$ and $\boldsymbol{r}^{B,p}_{tr_2,\omega_n}$ are the projection spaces corresponding to the projection matrices in $\boldsymbol{P}^A_{tr_2,\omega_l}$ and $\boldsymbol{P}^B_{tr_1,\omega_m}$, respectively, and are defined in (26) and (27), respectively as:

$$\boldsymbol{r}^{A,p}_{tr_1,\omega_k} = \boldsymbol{y}_A - \sqrt{\frac{\rho}{2}}\boldsymbol{h}^A_{tr_1,\omega_k}\hat{z}^p_{u_1} \quad (26)$$

$$\boldsymbol{r}^{B,p}_{tr_2,\omega_n} = \boldsymbol{y}_B - \sqrt{\frac{\rho}{2}}\boldsymbol{h}^B_{tr_2,\omega_n}\hat{z}^p_{u_2} \quad (27)$$

however, if $\hat{z}^p_{u_1} \neq x_{p_1}$ and $\hat{z}^p_{u_2} \neq x_{p_2}$, (25) yields [5], [9], [14]:

$$\sqrt{\frac{\rho}{2}}\boldsymbol{P}^A_{tr_2,\omega_l}\boldsymbol{h}^A_{tr_1,\omega_k}\left(x_{p_1} - \hat{z}^p_{u_1}\right) + \boldsymbol{P}^B_{tr_1,\omega_m}\boldsymbol{h}^B_{tr_2,\omega_n}\left(x_{p_2} - \hat{z}^p_{u_2}\right) + \boldsymbol{P}^A_{tr_2,\omega_l}\boldsymbol{n}_A + \boldsymbol{P}^B_{tr_1,\omega_m}\boldsymbol{n}_B \quad (28)$$

As can be seen from (21) , (24), (25) and (28), the Frobenius norms of (21) and (25) is less than (24) and (28), respectively. Hence, the most likely candidates of the transmitted symbols x_{p_1}, x_{p_2}, x_{q_1} and x_{q_2} are chosen by selecting the f_1 and f_2 most likely symbols, which offer the least Frobenius norms. Then, the ML rule is employed to perform an exhaustive search over the f_1 and f_2 selected most likely candidates, in order to estimate the transmitted APM symbols.

The steps following outlines the algorithm for the proposed orthogonal projection-based low-complexity detector of MBSTBC-SM-LD.

Firstly, the projection matrices for the τ-th, $\tau \in [1:c]$ antenna pair and for the time-slots A and B, given as $\boldsymbol{P}^{\tau,A}_{tr_1,\omega_k}$, $\boldsymbol{P}^{\tau,A}_{tr_2,\omega_l}$, $\boldsymbol{P}^{\tau,B}_{tr_1,\omega_m}$ and $\boldsymbol{P}^{\tau,B}_{tr_2,\omega_n}$ are obtained. Furthermore, the projection spaces $\boldsymbol{r}^{\tau,A,p}_{tr_1,\omega_k}$, $\boldsymbol{r}^{\tau,A,q}_{tr_2,\omega_l}$ $\boldsymbol{r}^{\tau,B,p}_{tr_2,\omega_n}$ and $\boldsymbol{r}^{\tau,A,q}_{tr_1,\omega_m}$ are also determined where $p,q \in [1:M]$, $\omega_k,\omega_l,\omega_m,\omega_n \in [1:N_m]$.

The projection matrices $\boldsymbol{P}^{\tau,A}_{tr_1,\omega_k}$ and $\boldsymbol{P}^{\tau,A}_{tr_2,\omega_l}$ of the proposed MBSTBC-SM-LD, for the τ-th antenna, during time-slot A, may be defined as [5], [14]:

$$\boldsymbol{P}^{\tau,A}_{tr_1,\omega_k} = \boldsymbol{I}_{N_r} - \boldsymbol{h}^{\tau,A}_{tr_1,\omega_k}\left(\left(\boldsymbol{h}^{\tau,A}_{tr_1,\omega_k}\right)^H \boldsymbol{h}^{\tau,A}_{tr_1,\omega_k}\right)^{-1}\left(\boldsymbol{h}^{\tau,A}_{tr_1,\omega_k}\right)^H \tag{29}$$

$$\boldsymbol{P}^{\tau,A}_{tr_2,\omega_l} = \boldsymbol{I}_{N_r} - \boldsymbol{h}^{\tau,A}_{tr_2,\omega_l}\left(\left(\boldsymbol{h}^{\tau,A}_{tr_2,\omega_l}\right)^H \boldsymbol{h}^{\tau,A}_{tr_2,\omega_l}\right)^{-1}\left(\boldsymbol{h}^{\tau,A}_{tr_2,\omega_l}\right)^H \tag{30}$$

while the projection matrices for time-slot B, $\boldsymbol{P}^{B}_{tr_1,\omega_m}$ and $\boldsymbol{P}^{B}_{tr_2,\omega_n}$ may be represented as:

$$\boldsymbol{P}^{\tau,B}_{tr_1,\omega_m} = \boldsymbol{I}_{N_r} - \boldsymbol{h}^{\tau,B}_{tr_1,\omega_m}\left(\left(\boldsymbol{h}^{\tau,B}_{tr_1,\omega_m}\right)^H \boldsymbol{h}^{\tau,B}_{tr_1,\omega_m}\right)^{-1}\left(\boldsymbol{h}^{\tau,B}_{tr_1,\omega_m}\right)^H \tag{31}$$

$$\boldsymbol{P}^{\tau,B}_{tr_2,\omega_n} = \boldsymbol{I}_{N_r} - \boldsymbol{h}^{\tau,B}_{tr_2,\omega_n}\left(\left(\boldsymbol{h}^{\tau,B}_{tr_2,\omega_n}\right)^H \boldsymbol{h}^{\tau,B}_{tr_2,\omega_n}\right)^{-1}\left(\boldsymbol{h}^{\tau,B}_{tr_2,\omega_n}\right)^H \tag{32}$$

The projection spaces for the τ-th transmit antenna pair of the proposed MBSTBC-SM-LD may be formulated as [5], [14]:

$$\boldsymbol{r}^{\tau,A,q}_{tr_2,\omega_l} = \boldsymbol{y}_A - \sqrt{\frac{\rho}{2}}\boldsymbol{h}^{\tau,A}_{tr_2,\omega_l}\hat{z}^{q}_{u_1} \tag{33}$$

$$\boldsymbol{r}^{\tau,B,q}_{tr_1,\omega_m} = \boldsymbol{y}_B - \sqrt{\frac{\rho}{2}}\boldsymbol{h}^{\tau,B}_{tr_1,\omega_m}\hat{z}^{q}_{u_2} \tag{34}$$

$$\boldsymbol{r}^{\tau,A,p}_{tr_1,\omega_k} = \boldsymbol{y}_A - \sqrt{\frac{\rho}{2}}\boldsymbol{h}^{\tau,A}_{tr_1,\omega_k}\hat{z}^{p}_{u_1} \tag{35}$$

$$\boldsymbol{r}^{\tau,B,p}_{tr_2,\omega_n} = \boldsymbol{y}_B - \sqrt{\frac{\rho}{2}}\boldsymbol{h}^{\tau,B}_{tr_2,\omega_n}\hat{z}^{p}_{u_2} \tag{36}$$

where $\boldsymbol{h}^{\tau,A}_{tr_1,\omega_k}$ and $\boldsymbol{h}^{\tau,A}_{tr_2,\omega_l}$ are the ω_k-th and ω_l-th, column vectors of the τ-th antenna pair channel matrices $\boldsymbol{H}^{\tau,A}_{tr_1}$ and $\boldsymbol{H}^{\tau,A}_{tr_2}$, respectively, which are employed during time slot A. The channel subspace $\boldsymbol{h}^{\tau,B}_{tr_1,\omega_m}$ and $\boldsymbol{h}^{\tau,B}_{tr_2,\omega_n}$ are the ω_m-th and ω_n-th column vectors of the channel matrices $\boldsymbol{H}^{\tau,B}_{tr_1}$ and $\boldsymbol{H}^{\tau,B}_{\tau,tr_2}$, respectively, which are the channel matrices for the τ-th antenna pair, employed during time-slot B.

Secondly, the f_1 and f_2 nearest estimates of x_{p_1} and x_{q_1}, $\boldsymbol{z}^{\tau}_{p_1} = \left[\hat{z}^{\tau,p}_1 \;\; \hat{z}^{\tau,p}_2 \;\; \cdots \;\; \hat{z}^{\tau,p}_{f_1}\right]$ and $\boldsymbol{z}^{\tau}_{q_1} = \left[\hat{z}^{\tau,q}_1 \;\; \hat{z}^{\tau,q}_2 \;\; \cdots \;\; \hat{z}^{\tau,q}_{f_2}\right]$ for the τ-th, $\tau \in [1:c]$ transmit antenna pair and the N_m^2 MAP combinations are obtained, and may be formulated as [5], [9]:

$$\hat{z}^{\tau,p}_{u_1} = \underset{\substack{\boldsymbol{r}^{A}_{tr_1,p,\omega_k},\\ \boldsymbol{r}^{B}_{tr_2,p,\omega_n}}}{\operatorname{argmin}}\left\{\left\|\boldsymbol{P}^{\tau,A}_{tr_1,\omega_k}\boldsymbol{r}^{\tau,A,q}_{tr_2,\omega_l}\right\| + \left\|\boldsymbol{P}^{\tau,B}_{tr_2,\omega_n}\boldsymbol{r}^{\tau,B,q}_{tr_1,\omega_m}\right\|^2_F\right\} \tag{37}$$

$$\hat{z}^{\tau,q}_{u_2} = \underset{\substack{\boldsymbol{r}^{A}_{tr_2,q,\omega_l},\\ \boldsymbol{r}^{B}_{tr_1,q,\omega_m}}}{\operatorname{argmin}}\left\{\left\|\boldsymbol{P}^{\tau,A}_{tr_2,\omega_l}\boldsymbol{r}^{\tau,A,p}_{tr_1,\omega_k}\right\| + \left\|\boldsymbol{P}^{\tau,B}_{tr_1,\omega_m}\boldsymbol{r}^{\tau,B,p}_{tr_2,\omega_n}\right\|^2_F\right\} \tag{38}$$

where $\tau \in [1:c]$, $\omega_k,\omega_l,\omega_m,\omega_n \in [1:N_m]$, $p,q \in [1:M]$. Finally, the joint ML rule is applied over all the $\boldsymbol{z}^{\tau,p}_{u_1}$ and $\boldsymbol{z}^{\tau,q}_{u_2}$ results obtained in (37) and (38), for all the c transmit antenna pair combinations and the N_m^2 MAP combinations. The joint ML detector for Scheme 1 and 3 may be represented as:

$$\begin{aligned}&[\hat{\tau},\hat{\omega}_k,\hat{\omega}_l,\hat{p},\hat{q}]\\ &= \underset{\boldsymbol{z}^{\tau}_{p},\boldsymbol{z}^{\tau}_{q}}{\operatorname{argmin}}\left\{\left\|\boldsymbol{y}_A - \sqrt{\frac{\rho}{2}}\left(\boldsymbol{h}^{\tau,A}_{tr_1,\omega_k}\hat{z}^{\tau,p}_{u_1} + \boldsymbol{h}^{\tau,A}_{tr_2,\omega_l}\hat{z}^{\tau,q}_{u_1}\right)\right\|^2_F\right.\\ &\quad\left. + \left\|\boldsymbol{y}_B - \sqrt{\frac{\rho}{2}}\left(\boldsymbol{h}^{\tau,B}_{tr_1,\omega_m}\hat{z}^{\tau,q}_{u_2} + \boldsymbol{h}^{\tau,B}_{tr_2,\omega_n}\hat{z}^{\tau,p}_{u_2}\right)\right\|^2_F\right\}\end{aligned} \tag{39}$$

where $\tau \in [1:c]$, $u_1 \in [1:f_1]$ and $u_2 \in [1:f_2]$.

VI. COMPUTATIONAL COMPLEXITY ANALYSIS

This section analyses the computational complexity in terms of complex operations performed by the proposed MBSTBC-SM-LD, Furthermore, we compare the MBSTBC-SM-LD with MBSTBC-SM.

In (10), each term contains ten N_R complex operations. Since the ML search is performed over N_m^2 MAP combinations, c transmit antenna pairs and M^2 symbol combination pairs, ignoring the real operations performed by the proposed system, the computational complexity may be given as:

$$10cN_RN_m^2M^2 \tag{40}$$

The computational complexity of the proposed MBSTBC-SM-LD is calculated in three phases.

Firstly, the computational complexity employed in calculating the projection matrix is similar to [5], hence, the computational complexity for the first phase of detection Δ_{phase_1}, may be given as:

$$\Delta_{phase_1} = 8N_R^2 + 12N_R - 4 \tag{41}$$

The second phase of detection Δ_{phase_2}, involves determining the most-likely symbol set $\hat{z}_{u_1}^{\tau;p}$ and $\hat{z}_{u_2}^{\tau;q}$ that has been transmitted, as given in (37) and (38). The computational complexity of Δ_{phase_2}, is given as:

$$\Delta_{phase_2} = 4(2MN_R^2 + 4MN_R + N_R - M) \quad (42)$$

It must be noted that the operations in (41) and (42) are performed across c transmit antenna pairs and N_m^2 MAP combination.

Thirdly, the computational complexity employed to perform an exhaustive ML search across the f_1 and f_2 most-likely candidate sets is similar to the computational complexity given in (40), however, instead of the M^2 symbol search, it reduces to $f_1 f_2$ symbol search. Hence, the computational complexity involved in searching the f_1 and f_2 symbol sets becomes:

$$\Delta_{phase_3} = 10cN_R f_1 f_2 N_m^2 \quad (43)$$

The total computational complexity for the low-complexity detector is the sum of the computational complexity for the three phases, viz; Δ_{phase_1}, Δ_{phase_2} and Δ_{phase_3}. The computational complexity is given as:

$$2cN_m^2 \left(4MN_R^2 + 8MN_R + 2N_R - 2M + 4N_R^2 + 6N_R + 5N_R f_1 f_2 - 2\right) \quad (44)$$

A summary of the computational complexities of the ML detector (MLD) and the low-complexity detector (LCD) is presented in Table 3. The computational complexities are calculated for $M = 16$ and 64, while in both cases, arbitrary values are chosen for f_1 and f_2, which offer very close error performance to the MLD. Furthermore, the percentage reduction in computational complexity, in terms of the number of complex multiplication, of the LC detector is compared with the ML detector, for a specified spectral efficiency (SE).

TABLE 3. Comparison of MBSTBC-SM-LD computational complexity for ML with low-complexity detector for $N_T = 4$ and $c = 4$

CONFIGURATION	SE	MLD	LCD	Reduction
16-QAM $N_R = 4, m_{rf} = 2$ $f_1 = 6, f_2 = 6$	7	655,360	296,704	54.72%
64-QAM $N_R = 2, m_{rf} = 1$ $f_1 = 30, f_2 = 30$	8	1,310,720	350,400	73.27%

VII. NUMERICAL RESULTS

In this section, the numerical results of the Monte-Carlo simulations for MBSTBC-SM and the proposed MBSTBC-SM-LD are compared for $M = 16$ and 64, employing Scheme 1 and 3. Furthermore, the numerical results of the reduced computational complexity detector which offer very close error performance with the optimal-ML detector over a fast, frequency-flat Rayleigh fading channel are presented. For our simulation, we assume that the channel is fully known by the receiver.

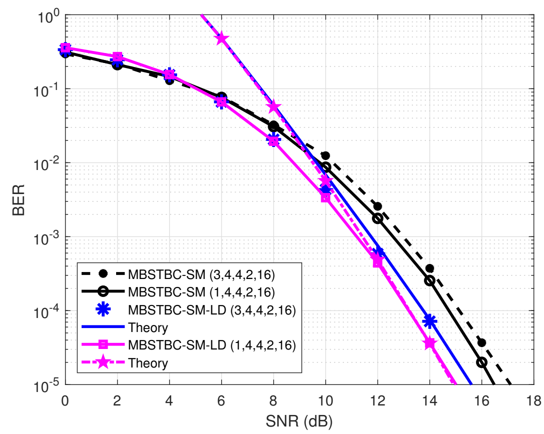

FIGURE 5. BER performance of MBSTBC-SM-LD and MBSTBC-SM for Schemes 1 and 3 versus SNR in dB.

In Figure 5, the average bit error rate (BER) performances of the different schemes of MBSTBC-SM-LD are compared with the BER performances of Scheme 1 and 3 of MBSTBC-SM employing $m_{rf} = 2$ RF mirrors, $M = 16$-QAM for Scheme 1 and 3. The notation (Scheme, N_T, N_R, m_{rf}, M) has been employed for Figure 5 and 6, where N_T is the number of transmit antennas, N_R is the number of receive antennas, m_{rf} is the number of RF mirrors and M is the constellation size of the graycoded M-ary QAM constellation. The legend for the numerical values of the union-bound on the ABEP of the MBSTBC-SM-LD system is given directly below the respective MBSTBC-SM-LD as "Theory" for Figures 5 and 6.

Considering Figure 5, the theoretical expression, on the union-bound of the ABEP of MBSTBC-SM-LD given in (18) is evaluated and is compared with the simulated results. As

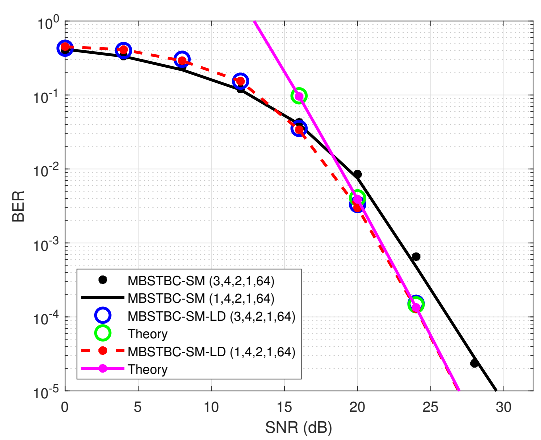

FIGURE 6. BER performance of MBSTBC-SM-LD and MBSTBC-SM for Schemes 1 and 3 versus SNR in dB.

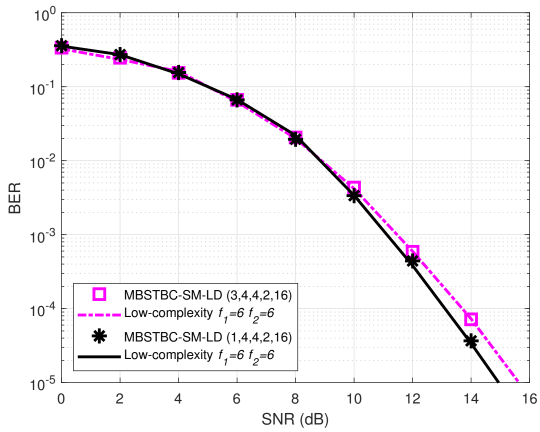

FIGURE 7. BER comparison of ML and low-complexity detector for 16-QAM

expected, the theoretical values of the proposed MBSTBC-SM-LD demonstrates a tight match with the simulated ABEP at higher SNR. Furthermore, the proposed MBSTBC-SM-LD demonstrates a superior error performance over MBSTBC-SM. For example, the Scheme 1 of MBSTBC-SM-LD outperforms Scheme 1 and Scheme 3 of MBSTBC-SM by 1.5 and 2 dB gain, respectively, when the BER is 10^{-5}. Furthermore, Scheme 3 of the proposed MBSTBC-SM-LD outperforms Scheme 1 and Scheme 3 of MBSTBC-SM by 1 and 1.5 dB, respectively.

Comparing the different MBSTBC-SM-LD schemes, Scheme 1 of MBSTBC-SM-LD demonstrates a better performance than Scheme 3. For example, Scheme 1 shows a 0.5 dB gain over Scheme 3 of MBSTBC-SM-LD.

Referring to Figure 6, the theoretical results for MBSTBC-SM-LD demonstrate a tight match with the simulated equivalent at high SNR. However, there is a close match between scheme 1 and scheme 3 of MBSTBC-SM-LD $m_{rf} = 1$ and $M = 64$-QAM. For example, at a BER of 10^{-5}, the difference in BER between Scheme 1 and Scheme 3 is negligible

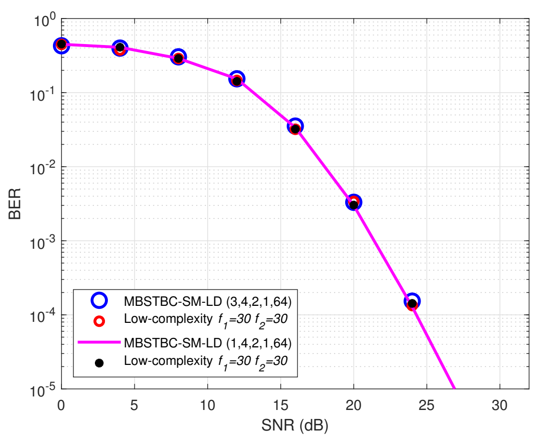

FIGURE 8. BER comparison of ML and low-complexity detector for 64-QAM

as there is a tight match between both schemes. Furthermore, the MBSTBC-SM-LD scheme demonstrate significant improvement over MBSTBC-SM, for example, the MBSTBC-SM-LD schemes outperforms the MBSTBC-SM schemes by ≈ 2.5 dB gain in SNR, when the BER is 10^{-5}.

In Figures 7 and 8, the BER performances of the optimal ML detector for MBSTBC-SM-LD are compared with the BER performances of the low-complexity near-ML detector for MBSTBC-SM-LD. Similar to Figure 5 and 6, the notation (Scheme, N_T, N_R, m_{rf}, M) has been employed for Figure 7 and 8 also, where N_T is the number of transmit antennas, N_R is the number of receive antennas, m_{rf} is the number of RF mirrors and M is the constellation size of the graycoded M-ary QAM constellation. Furthermore, the corresponding low-complexity near-ML detector of MBSTBC-SM-LD, which employs f_1 and f_2 most likely candidates, is given directly below the individual optimal ML detector of MBSTBC-SM-LD. From the different graphs in Figures 7 and 8, the low-complexity detector shows a tight match with its counterpart optimal near-ML detector with high reduction in computational complexity under the same channel condition.

VIII. CONCLUSION

In this paper, we have proposed the application of labelling diversity to MBSTBC-SM. Two schemes were proposed for MBSTBC-SM-LD, viz., Scheme 1 and Scheme 3. Both schemes of MBSTBC-SM-LD have demonstrated significant improvement over MBSTBC-SM. Furthermore, a theoretical expression for the union-bound on the ABEP of MBSTBC-SM-LD was formulated and agrees well with the numerical values of the Monte Carlo simulations for MBSTBC-SM-LD. Finally, a low-complexity near-ML detector which is based on orthogonal projection was proposed. A 73% reduction in computational complexity is achieved by the low-complexity detector when compared to the optimal ML detector of MBSTBC-SM-LD, especially at high SNR for $M = 64$-QAM.

REFERENCES

[1] S. M. Alamouti, "A simple transmit diversity technique for wireless communications," IEEE Journal on Selected Areas in Communications, vol. 16, no. 8, pp. 1451–1458, 1998.
[2] V. Tarokh, H. Jafarkhani, and A. R. Calderbank, "Space-time block coding for wireless communications: performance results," IEEE Journal on selected areas in communications, vol. 17, no. 3, pp. 451–460, 1999.
[3] R. Y. Mesleh, H. Haas, S. Sinanovic, C. W. Ahn, and S. Yun, "Spatial modulation," IEEE Transactions on vehicular technology, vol. 57, no. 4, pp. 2228–2241, 2008.
[4] E. Basar, U. Aygolu, E. Panayirci, and H. V. Poor, "Space-time block coded spatial modulation," IEEE transactions on communications, vol. 59, no. 3, pp. 823–832, 2010.
[5] K. Govindasamy, H. Xu, and N. Pillay, "Space-time block coded spatial modulation with labeling diversity," International Journal of Communication Systems, vol. 31, no. 1, p. e3395, 2018.
[6] N. Pillay and H. Xu, "Uncoded space-time labeling diversity-Application of media-based modulation with rf mirrors," IEEE Communications Letters, vol. 22, no. 2, pp. 272–275, 2018.
[7] E. Seifi, M. Atamanesh, and A. K. Khandani, "Media-based MIMO: A new frontier in wireless communications," arXiv preprint arXiv:1507.07516, 2015.

[8] B. S. Adejumobi, N. Pillay, and S. H. Mneney, “A study of spatial media-based modulation using RF mirrors,” in IEEE AFRICON, Sep. 2017, pp. 336–341.

[9] B. S. Adejumobi and N. Pillay, “RF mirror media-based space-time block coded spatial modulation techniques for two time-slots,” IET Communications, vol. 13, no. 15, pp. 2313–2321, 2019.

[10] Y. Naresh and A. Chockalingam, “On media-based modulation using RF mirrors,” IEEE Transactions on Vehicular Technology, vol. 66, no. 6, pp. 4967–4983, 2016.

[11] E. Basar and I. Altunbas, “Space-time channel modulation,” IEEE Transactions on Vehicular Technology, vol. 66, no. 8, pp. 7609–7614, 2017.

[12] H. Xu, K. Govindasamy, and N. Pillay, “Uncoded space-time labeling diversity,” IEEE Communications Letters, vol. 20, no. 8, pp. 1511–1514, 2016.

[13] I. Al-Shahrani, “Performance of M-QAM over generalized mobile fading channels using mrc diversity,” MS thesis, 2007.

[14] S. Bahng, S. Shin, and Y. O. Park, “ML approaching MIMO detection based on orthogonal projection,” IEEE Communication Letters, vol. 11, no. 6, pp. 474–476, 2007.

BABATUNDE S. ADEJUMOBI Babatunde Segun Adejumobi received B.Sc. and M.Sc. degree in Electronic and Computer Engineering from the Lagos State University, Lagos, Nigeria in 2007 and 2012, respectively. Dr. Adejumobi obtained his Ph.D. in Electronic Engineering (Wireless Communication) from the Department of Electrical, Electronic and Computer Engineering of the University of KwaZulu-Natal, Durban, South Africa. His current research includes spatial modulation, space-time block coded modulation and orthogonal frequency division multiplexing. However, he also has interest in optical communication, wireless communications and Image processing.

THOKOZANI SHONGWE received the B. Eng degree in Electroinc engineering from the University of Swaziland, Swaziland, in 2004 and the M.Eng degree in Telecommunications Engineering from the University of the Witwatersrand, South Africa, in 2006 and the D. Eng degree from the University of Johannesburg, South Africa, in 2014. He is currently an Associate Professor at the University of Johannesburg, department of electrical and electronic engineering Technology. He is a recipient of the 2014 University of Johannesburg Global Excellence Stature (GES) award, which was awarded to him to carry out his postdoctoral research at the University of Johannesburg. In 2016, Prof T. Shongwe was a recipient of the TWAS-DFG Cooperation Visits Programme funding to do research in Germany. Other awards that he has received in the past are: the post-graduate merit award scholarship to pursue his master's degree at the University of the Witwatersrand in 2005, which is awarded on a merit basis; In the year 2012, Prof. Shongwe (and his co-authors) received an award of the best student paper at the IEEE ISPLC 2012 (power line communications conference) in Beijing, China. Prof T. Shongwe's research fields are in Digital Communications and Error Correcting Coding. His research interests are in power-line communications; cognitive radio; smart grid; visible light communications.